ACS Catalysis

Research Article

pubs.acs.org/acscatalysis

# Acetic Acid Reforming over Rh Supported on $La_2O_3/CeO_2–ZrO_2$: Catalytic Performance and Reaction Pathway Analysis

Angeliki A. Lemonidou,*[,†] Ekaterini C. Vagia,[†] and Johannes A. Lercher[‡,§]

[†]Department of Chemical Engineering, Aristotle University of Thessaloniki, University Campus, GR-54124 Thessaloniki, Greece

[‡]Institute for Integrated Catalysis, Pacific Northwest National Laboratory, 902 Battelle Boulevard, Richland, Washington 99352, United States

[§]Department of Chemistry and Catalysis Research Center, Technische Universität München, Lichtenbergstrasse 4, 85748 Garching, Germany

**ABSTRACT:** Reforming of acetic acid was investigated on Rh supported on $CeO_2–ZrO_2$ modified with 3 wt % La. The active catalyst converted acetic acid to $H_2$-rich gas and hardly formed coke. The low rate of coke formation is concluded to be related to the presence of redox-active oxygen limiting the concentration of coke precursors. Temperature-programmed $^{18}O_2$ isotope exchange measurements showed that the $La_2O_3$ and Rh enhanced the mobility of lattice oxygen compared with that of the parent $CeO_2–ZrO_2$. Ketonization and decarboxylation of acetic acid are the dominating reactions over the latter up to 600 °C, whereas above 600 °C, steam reforming and water gas shift also contribute. Over 0.5 wt % Rh on $La_2O_3/CeO_2–ZrO_2$, reforming and water gas shift reactions dominate, even below 300 °C, producing mostly $H_2$ and $CO_2$. Using isotope labeling, it is shown that acetic acid adsorbs dissociatively on Rh, forming acetates, which sequentially decarboxylate and form surface methyl groups. The latter are in turn converted to CO, $CO_2$, and $H_2$.

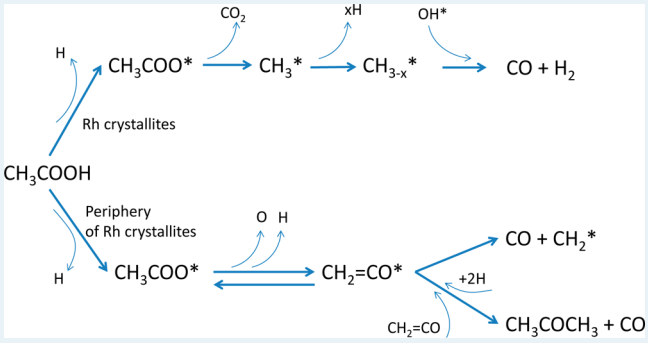


**KEYWORDS:** *hydrogen production, steam reforming, acetic acid, $La_2O_3/CeO_2–ZrO_2$, supported Rh*

## 1. INTRODUCTION

The need for $H_2$ production in biorefineries is expected to be high, as large quantities need to be available for the hydrogenations of intermediates and final products.[1] $H_2$ can be produced from biomass, mainly via two thermochemical processes: gasification and flash pyrolysis followed by steam reforming of the pyrolysis oil.[1−4] This pyrolysis oil (bio-oil) is a complex mixture consisting of acids, alcohols, aldehydes, esters, ketones, sugars, phenols, and multifunctional compounds.[5,6] Steam reforming can be used to convert the entire bio-oil or mostly the hydrophilic light fraction to a $H_2$-rich stream.[7] The latter option seems to have higher potential for industrial development because in such a case, $H_2$ produced from the hydrophilic part of the bio-oil can be directly used for the selective HDO of the heavier hydrophobic part, thus improving the economics of the bio-oil upgrading.

Our previous studies on the thermodynamic equilibrium of steam and autothermal reforming of model compounds of bio-oil, acetic acid, ethylene glycol, and acetone demonstrated that the oxygenates in the presence of steam are converted to $H_2$-rich mixtures achieving maximum $H_2$ yields of over 80% at 650 °C without carbon deposition under atmospheric pressure and steam/carbon ratios above 1.[8,9]

Acetic acid is one of the major components of bio-oil and is, therefore, considered a representative model compound. Steam reforming of acetic acid has been the subject of many studies exploring the role of the metal and the support on the activity and $H_2$ selectivity.[10−22] The high tendency of the thermally unstable oxygenates to decompose forming carbonaceous deposits, however, has been recognized to be the main obstacle for scaling up.[12,13,22] As a consequence, the resistance of $CeO_2–ZrO_2$ to coking in reforming reactions has attracted attention in recent years. Partial oxidation, $CO_2$ reforming, and steam reforming of methane using Ni and Pt over $CeO_2–ZrO_2$, $CeO_2$, and $ZrO_2$ have been widely examined.[23−30] $CeO_2–ZrO_2$ has also been investigated in phenol and ethanol reforming,[31−35] but it has received less attention for steam reforming of bio-oil and its components.[18,36,37]

Our recent results[37] with Ni and Rh supported on $CeO_2–ZrO_2$ suggest that these catalysts are active and selective to reform acetic acid with yields approaching thermodynamic equilibrium above 650 °C. The concentration of coke was very low, especially in the presence of the $Rh/CeO_2–ZrO_2$. However, a moderate (20%) loss of activity was observed after 15 h on stream, attributed to catalyst sintering.

**Received:** April 23, 2013
**Revised:** July 10, 2013
**Published:** July 11, 2013

   dx.doi.org/10.1021/cs4003063 | *ACS Catal.* 2013, 3, 1919−1928

In an attempt to overcome the problem of catalyst sintering, we modified the support by adding small amounts of $La_2O_3$, which has been reported to increase the support stability.[38,39] We report here activity, selectivity, and stability of such Rh/$La_2O_3$/$CeO_2$−$ZrO_2$ catalyst for acetic acid steam reforming. Temperature-programmed surface reaction and isotope labeling is used to investigate the reaction paths on this catalyst in comparison with the parent, not stabilized, material.

## 2. EXPERIMENTAL SECTION

**2.1. Catalyst Preparation.** The wet impregnation method was applied for the preparation of catalyst. Cerium-doped zirconium hydroxide provided by Mel Chemicals (XZO802) was calcined at 800 °C for 4 h. The calcined material with a composition $CeO_2/ZrO_2$ = 15/85 (wt) was used as the support. The latter was impregnated with an aqueous solution of $La(NO_3)_3{\cdot}6H_2O$ followed by the removal of water in vacuum. The material was dried overnight at 120 °C and then calcined in air at 400 °C for 2 h. The $La_2O_3$-modified support was impregnated with $RhCl_3{\cdot}3H_2O$ following the procedure described for $La(NO_3)_3{\cdot}6H_2O$. The final material contained 3wt % La and 0.5 wt % Rh. Before the reforming experiments, the catalyst was reduced at 750 °C for l hour in 25 vol % $H_2$/He flow.

**2.2. Catalyst Characterization.** The surface area of the materials was measured by $N_2$ adsorption at 77 K using the multipoint BET analysis method with an Autosorb-1 Quantachrome flow apparatus. X-ray diffraction (XRD) patterns were obtained using a Siemens D500 diffractometer, with Cu K$\alpha$ radiation.

$NH_3$ temperature-programmed desorption (TPD-$NH_3$) was used to determine the acidic properties of the catalyst. The experiments were performed in a gas flow system using a U-tube reactor connected online with a quadrupole mass analyzer (Omnistar, Balzers). The samples (200 mg) were pretreated at 650 °C for 0.5 h and then cooled to 100 °C under He flow. The pretreated samples were saturated with 5% $NH_3$/He for 1 h at 100 °C, with subsequent flushing with He at 100 °C for 1 h to remove the physisorbed ammonia. TPD analysis was carried out from 100 to 700 °C at a heating rate of 10 °C/min. Quantitative analysis of the desorbed ammonia was based on ($m/z$) 15.

The metal dispersion was measured by temperature-programmed desorption of $H_2$ (TPD-$H_2$). Catalyst (300 mg) was treated at 600 °C for 1 h under 20% $O_2$/He flow, then cooled to 300 °C, and then reduced with 20% $H_2$/He for 1 h at 250 °C to reduce $RhO_x$ to metal Rh. The reduced sample was heated to 500 °C in He flow to desorb reversibly adsorbed $H_2$ and then cooled to room temperature. A flow of 5% $H_2$/He was applied for 30 min at room temperature, followed by He flow for another 30 min. The TPD analysis was carried out from room temperature to 700 °C at a heating rate 10 °C/min.

The oxygen mobility was examined with $O_2$ isotopic exchange experiments. The material (300 mg) was first reduced at 300 °C. Under these conditions, Rh is reduced while $CeO_2$ remains fully oxidized. After reduction, the sample was cooled in He flow to room temperature. The exchange with $^{18}O_2$ (2% $^{18}O_2$/He) was explored by increasing the temperature linearly from 50 to 750 °C at 15 °C/min. The signals at $m/z$ 32, 34, and 36 were monitored for the $^{16}O_2$, $^{16}O^{18}O$, and $^{18}O_2$, respectively.

The amount of solid carbon deposited on the catalyst after a fixed time of reforming tests was measured in a CHN stoichiometric analyzer LECO 800. The oxidation profile of the solid carbonaceous deposits was determined in a thermogravimetric unit (STD2960 TA Instruments). The used catalyst was heated to 1000 °C at a rate of 10 °C/min in air flow.

**2.3. Catalytic Testing.** *2.3.1. Steady State Tests.* The experiments were performed at atmospheric pressure in a laboratory unit equipped with a mass flow controlled system for gas admission, a fixed bed quartz reactor, and an online gas chromatograph. An HPLC pump (Gilson 350) was used for feeding the liquid reactants (mixture of acetic acid and water) via a preheater. The inlet flow of the liquid mixture was 0.1 $cm^3$/min. He was used as diluent at a flow of 100 $cm^3$/min. The fixed bed reactor was heated electrically by a tubular furnace, with three independently controlled temperature zones. The temperature in the middle of the catalytic bed was measured with a coaxial thermocouple. The hot gases exiting the reactor were cooled to condense the liquid products and the unconverted reactants. The gas phase products were analyzed with an online gas chromatograph (Varian 3700) equipped with TCD. To separate the gaseous products, two columns were used: Porapak Q for $CO_2$, $C_2H_4$, $C_2H_6$, and higher hydrocarbons and MS 5A for $H_2$, $O_2$, CO, and $CH_4$. The liquid products were analyzed offline in a gas chromatograph (Varian 3300) equipped with FID using an HP-FFAP column.

The performance of the catalyst was investigated under variable operating conditions such as temperature (550−750 °C) steam/carbon ratio (1.5−6) and the presence or absence of oxygen. In these tests, the gas hourly space velocity remained constant at 34 500 $h^{-1}$. This corresponds to a residence time of 5.5 ms. Time on-stream activity of the catalyst was examined at 650 °C, S/C = 3 and GHSV = 28 000 $h^{-1}$. In all tests, catalyst particles were diluted with quartz particles at a 1/2 (wt) ratio.

The terms conversion and product yield used to describe the catalytic results in reforming of the bio-oil components are presented in detail in our previous publication.[13] The selectivities of carbon-containing products CO, $CO_2$ $CH_4$, and $CH_3COCH_3$ were calculated on a C basis; that of $H_2$, on a H basis.

*2.3.2. Dynamic Transient Tests.* Dynamic transient tests were conducted in a fast response flow unit.[40] Admission of water and acetic acid to the reactor was attained with Ar flow passing through a saturator containing water and acetic acid. The reactant gas molar composition was ∼0.75−1% acetic acid; 4.5−6% steam (S/C = 3); and the rest, argon. Temperature varied from 50 to 800 °C at a ramp rate of 15 °C/min. In the tests with deuterated acetic acid ($CH_3COOD$ and $CD_3COOD$), the same conditions were applied. The gas phase composition at the reactor outlet was calculated on the basis of the mass spectrometer signals at various $m/e$ ratios. The responses of mass spectrometer were calibrated with mixtures of known concentrations of reactants and products.

## 3. RESULTS AND DISCUSSION

**3.1. Characterization of the Catalysts.** The main chemical and physicochemical properties of the catalyst and the support are compiled in Table 1. The catalyst shows a slightly lower surface area than that of bare support before the depositions and calcinations (compare 38.6 and 41.8 $m^2$/g). The only crystal phase present in the diffractograms (not shown) was that of the support, the mixed crystalline tetragonal phase of $Zr_{0.84}Ce_{0.16}O_2$. Indications for a La-containing crystalline phase were not observed, implying that the additive


dx.doi.org/10.1021/cs4003063 | ACS Catal. 2013, 3, 1919−1928

**Table 1. Physicochemical Characteristics of the Support and the Catalyst**

| | sample | |
|---|---|---|
| | $CeO_2$–$ZrO_2$ (support) | $Rh/La_2O_3/CeO_2$–$ZrO_2$ |
| metal/dopant, wt % | | 0.5(Rh), 3(La) |
| surface area, $m^2/g$ | 41.8 | 38.6 |
| crystal phase | $Zr_{0.84}Ce_{0.16}O_2$ | $Zr_{0.84}Ce_{0.16}O_2$ |
| metal dispersion | | 0.24 |
| acidity, mmol $NH_3/g$ | 0.09 | 0.10 |
| reduction temperature onset, °C | | |
| metal | | 150 |
| support | >450 | >350 |

is finely dispersed. Diffraction peaks of Rh were also not detected, as its concentration (0.5 wt %) is far below the detection limit.

The profiles of the $NH_3$ desorbing from the catalyst and the bare support as a function of temperature are shown in Figure 1. Both profiles are characterized by one broad peak centered

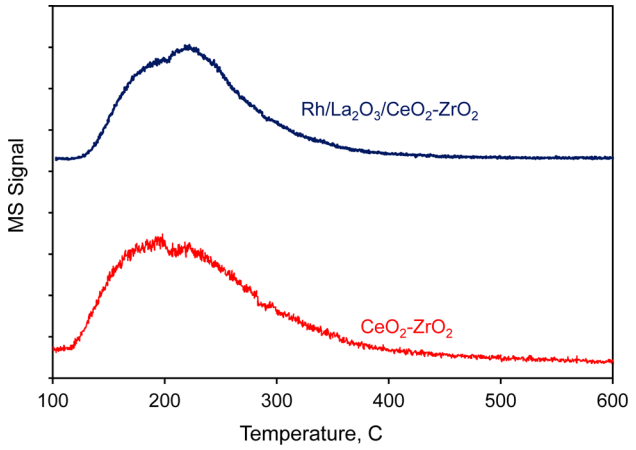


**Figure 1.** Temperature-programmed desorption of ammonia of $CeO_2$–$ZrO_2$ and $Rh/La_2O_3/CeO_2$–$ZrO_2$.

around 200 °C, indicative of the presence of acid sites of weak to medium strength. The presence of Rh and $La_2O_3$ does not seem to affect the acidic properties (Figure 1 and Table 1). However, $La_2O_3$ has an effect on metal distribution: it increases the dispersion of Rh (0.24) compared with that of the nonmodified $Rh/CeO_2$–$ZrO_2$ (0.12).[37]

The characteristic high mobility of lattice oxygen of $CeO_2$–$ZrO_2$ under reforming conditions is very important because O from the $CeO_2$ lattice oxidizes surface carbonaceous species. This mobility of lattice oxygen was investigated by $O_2$ isotope exchange, that is, temperature-programmed $^{18}O_2$ isotope exchange (TPIE) measurements. The profiles of $^{16}O_2$ and $^{18}O^{16}O$ evolving from the surface of the support and the catalyst as a function of temperature are presented in Figure 2. $CeO_2$–$ZrO_2$ starts to exchange lattice oxygen with the gaseous $^{18}O_2$ at 360 °C. At the initial steps of the exchange, the signal of $^{16}O_2$ dominates (Figure 2a). The release of $^{16}O_2$ indicates that the multiple heteroexchange mechanism prevails. The evolution of the cross-labeled oxygen $^{16}O^{18}O$ proceeds with lower rates and becomes significant at higher temperatures as the material is depleted in $^{16}O$, suggesting also the participation of the

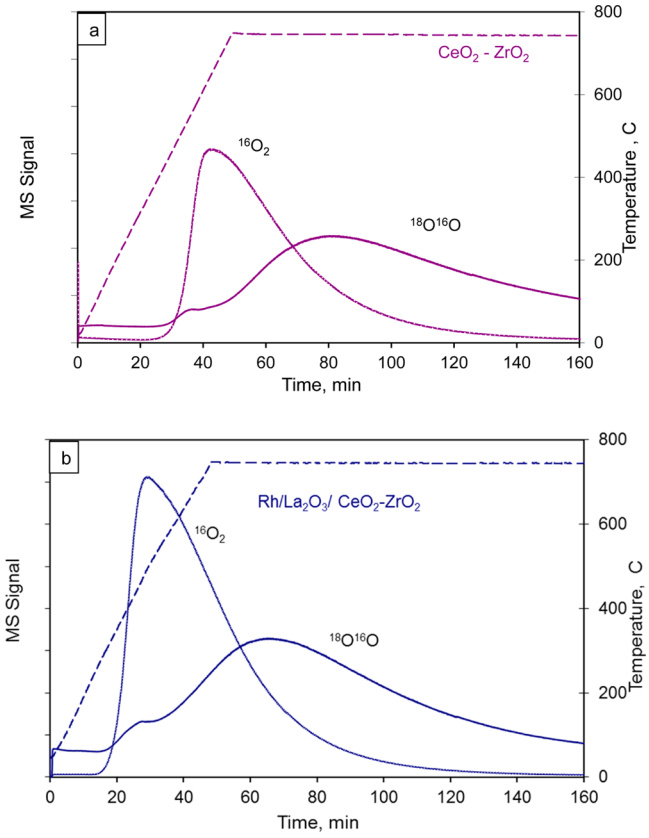


**Figure 2.** Temperature programmed treatment in $^{18}O_2$ flow of (a) $CeO_2$–$ZrO_{2l}$ and (b) $Rh/La_2O_3/CeO_2$–$ZrO_2$. Profiles of oxygen exchanged ($^{16}O_2$, $^{18}O^{16}O$).

simple heteroexchange mechanism. The exchange of labeled gas-phase oxygen with the lattice oxygen is referred to as heterolytic exchange and can occur via a simple (R1 mechanism, the exchange of only one surface oxygen species) and/or a multiple (R2 mechanism, the simultaneous exchange of two surface oxygen species) heteromolecular $^{18}O$ isotope exchange mechanism.[41,42]

The evolution of $^{16}O_2$ in the gas phase over $Rh/La_2O_3/CeO_2$–$ZrO_2$ starts at considerably lower temperature, around 260 °C (Figure 2b), suggesting that the joint presence of Rh and $La_2O_3$ facilitates the exchange of lattice oxygen, whereas $Rh/CeO_2$–$ZrO_2$ started to exchange at 330 °C.[37] As with the support, at low temperatures, the multiple heteroexchange mechanism prevails, but the simple mechanism dominates at high temperatures.

The exchange of $O_2$ is not limited to the outermost oxygen layer for both materials but extends significantly to the bulk. The concentration of total lattice oxygen $^{16}O$ exchanged for the support is 4.5 mmol/g, which corresponds to ~9 monolayers. For $Rh/La_2O_3/CeO_2$–$ZrO_2$, this concentration is significantly higher, 6.8 mmol/g, corresponding to 15 monolayers. The changes of the overall exchange rate of gaseous $^{18}O_2$ with varying temperatures (not shown) were used to calculate the apparent activation energy of the exchange process, leading to 115.4 kJ/mol for $CeO_2$–$ZrO_2$ and 72 kJ/mol for $Rh/La_2O_3/CeO_2$–$ZrO_2$. The respective activation energy of the unmodified $Rh/CeO_2$–$ZrO_2$ was 106 kJ/mol.[37] These values indicate that both Rh and $La_2O_3$ facilitate the exchange. The lower apparent energy of activation also shows not only that the better exchange is related to a higher dispersion of Rh, but also


dx.doi.org/10.1021/cs4003063 | ACS Catal. 2013, 3, 1919–1928

that the presence of $La_2O_3$ changes the reducibility of the support. In this context, it is interesting to note that $La_2O_3$ has been reported to increase the metal/support interaction in Pd/$CeO_2$ catalysts,[43] generating additional anion vacancies and favoring in this way bulk oxygen diffusion.[44,45] The increase in the metal support interaction of Rh/$La_2O_3$/$CeO_2$–$ZrO_2$ is shown here by the promotion of the $O_2$ exchange. The increase in the oxygen mobility facilitates the reduction of the support and, on the other hand, inhibits the reduction of the metal, stabilizing Rh in a positively charged state. Indeed, we observed a shift in the Rh reduction temperature from 100 °C in the unmodified catalyst[37] to 150 °C in Rh/$La_2O_3$/$CeO_2$–$ZrO_2$ (Table 1). The opposite trend was observed for the reduction of ceria, which was facilitated by the presence of $La_2O_3$, indicating the onset of the reduction temperature at 350 °C.

**3.2. Catalyst Performance under Steady State Conditions.** *3.2.1. Activity As a Function of Reaction Parameters.* Previous studies on the equilibrium compositions of an acetic acid–steam system under steam reforming conditions showed that acetic acid is fully converted, even at room temperature, to a mixture of $H_2$, $CO_2$, CO, and $CH_4$ at a steam/carbon ratio over 1 and atmospheric pressure.[8] Thermodynamically, the formation of solid carbon is not possible in the presence of excess steam (S/C > 1). The equilibrium molar composition of the gaseous products formed at 500–800 °C, of interest to the present experimental work, is presented by the dotted lines in Figure 3. The mixture is rich in

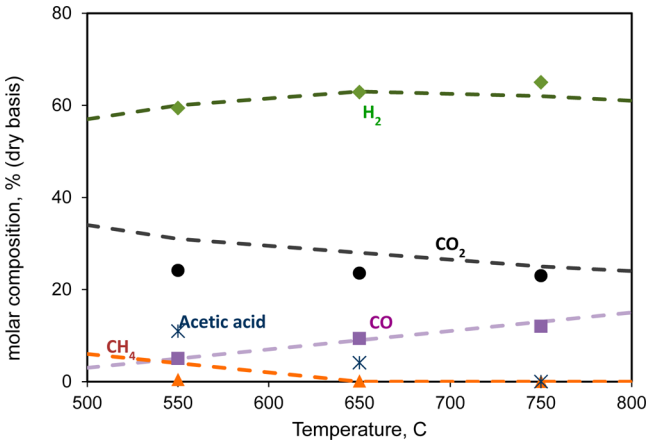


**Figure 3.** Steam reforming of acetic acid over Rh/$La_2O_3$/$CeO_2$–$ZrO_2$ catalyst(S/C = 3, GHSV = 34 500 $h^{-1}$). Effect of temperature on reactor exit steam composition. Equilibrium, dotted lines; experimental, symbols.

$H_2$, showing a maximum at 650 °C. At higher temperatures, the $H_2$ concentration starts decreasing. On the other hand, $CH_4$ appears at low concentrations and almost vanishes at temperatures over 650 °C. The prevailing carbon oxide is the $CO_2$ under all temperatures, but the share of CO increases steadily with temperature as a result of the WGS equilibrium.

The activity of the catalyst was explored as a function of temperature at 550, 650, and 750 °C using a steam-to-carbon ratio of 3 and a space velocity based on carbon of 34 500 $h^{-1}$. Acetic acid conversion increased with temperature approaching 100% at 750 °C. At 550 °C, the rate of acetic acid consumed per gram of catalyst is 0.12 mmol·$g^{-1}$·$s^{-1}$, which corresponds to an intrinsic rate per metal site (TOF) of almost 10 $s^{-1}$. It is interesting to note that these TOFs are significantly higher than the TOFs of various Ni-, Rh-, and Ru-based catalysts at 550 °C, which do not surpass 2 $s^{-1}$.[16,39]

The main products observed were $H_2$, $CO_2$, and CO. The catalyst is very selective to $H_2$, reaching values over 98% in the whole temperature range. This implies that the reforming activity of the catalyst is not limited to acetic acid, but also extends to the intermediate products. Methane and acetone formed via decarboxylation and ketonization, respectively, are almost fully reformed to hydrogen and carbon oxides under the reaction conditions used. The composition of the reactor effluent as a temperature function is presented in Figure 3 (symbols). At 550 and 650 °C, the composition slightly differs from the equilibrium values because there is still unconverted acetic acid, whereas under thermodynamic equilibrium conditions, all acetic acid should be converted. $H_2$ and CO follow the equilibrium under all temperatures, but the partial pressure of $CO_2$ is lower than expected from the thermodynamic equilibrium. The performance of the catalyst is similar to that of equilibrium at the highest temperature used, 750 °C. Measurable quantities to acetone and methane were observed only at the lowest reaction temperature.

The effect of the steam/carbon ratio was investigated by conducting tests at $H_2O$/C ratios 1.5, 3, and 6. The composition of the exit stream is presented in Figure 4,

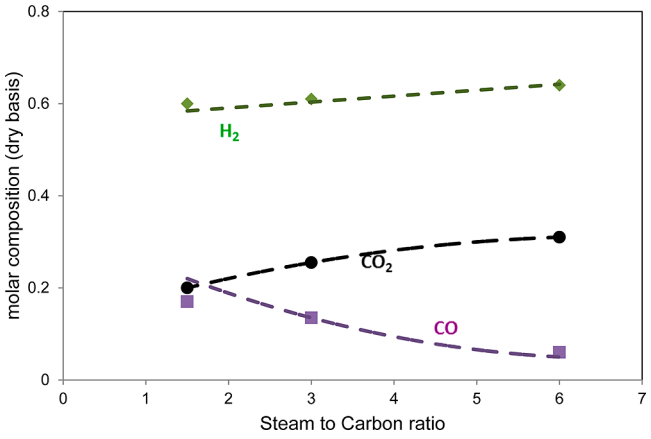


**Figure 4.** Steam reforming of acetic acid over Rh/$La_2O_3$/$CeO_2$–$ZrO_2$catalyst (temp = 750 °C, GHSV = 34 500 $h^{-1}$). Effect of steam-to-carbon ratio on reactor effluent composition. Equilibrium, dotted lines; experimental, symbols.

together with the respective equilibrium values. The equilibrium mixture is slightly enriched in $H_2$ (10% gain) with a S/C increase from 1.5 to 6. The increasing partial pressure of steam increases the ratio of $CO_2$/CO, indicating the importance of the water gas shift reaction. The experimental data under the three S/C ratios are similar to that of equilibrium, confirming that at 750 °C, the catalyst enables the gaseous product stream to be in equilibrium at moderate and high S/C ratios. The most pronounced effect of steam is related, however, to coke deposition, discussed in the next section.

According to thermodynamics, the amount of oxygen needed to attain autothermal conditions in the reformer in the 550–750 °C range, is around 0.3 mol $O_2$/mol acetic acid.[9] The effect of oxygen was also explored. In the tests conducted, apart from steam, oxygen was added to the feed stream in quantities sufficient to attain autothermicity. The presence of $O_2$ leads to higher activity because the conversion of acetic acid was complete, even at 550 °C. This is due to direct oxidation of


dx.doi.org/10.1021/cs4003063 | ACS Catal. 2013, 3, 1919–1928

acetic acid to $CO_2$ and $H_2O$. The consumption of part of the acetic acid to other than reforming reactions negatively affects the hydrogen yield, which did not exceed 70%.

*3.2.2. Catalyst Stability.* The stability of the catalyst was tested at 650 °C for 15 h TOS with a space velocity of 28 000 $h^{-1}$. The results are depicted in Figure 5. The loss in acetic acid

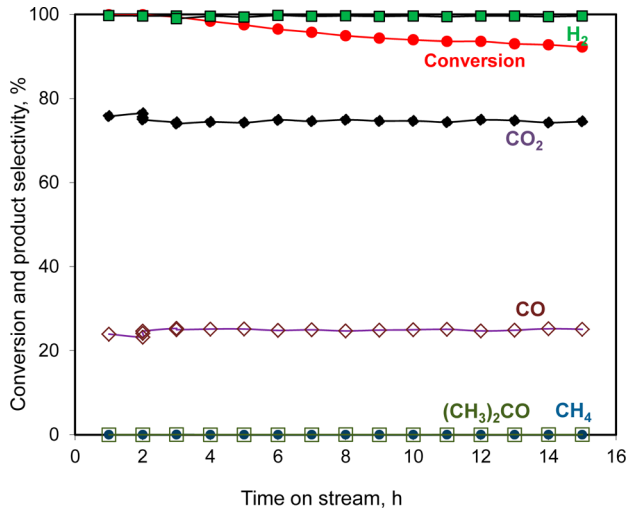


**Figure 5.** Steam reforming of acetic acid over $Rh/La_2O_3/CeO_2–ZrO_2$catalyst. Effect of reaction time on the catalyst performance (temp = 650 °C, S/C = 3, GHSV = 28 000 $h^{-1}$).

conversion is limited to 8%. The selectivity to the products formed remains unchanged during time on stream, confirming that the slight deactivation is solely related to the number of accessible sites. Time on-stream stability under similar operating conditions over Rh catalyst on undoped ceria–zirconia support resulted in 20% activity loss.[37] Coking and sintering, the main factors contributing to the loss of active sites, have been shown to be very limited. The presence of $La^{3+}$ stabilizes the support by inhibiting agglomeration, in agreement with the literature.[38,39,46–48] Coke deposited was also very low and will hardly affect the catalyst performance, as described below.

*3.2.3. Coke Deposition.* Coke deposition was investigated as a function of the steam-to-carbon ratio, presence of $O_2$ in the feed stream (oxidative autothermal reforming), and time on-stream. Except for the latter test, all others experiments were conducted at 750 °C for 3 h. Table 2 presents the results of coke produced in acetic acid reforming as the percentage of the C mol in the feedstock that are converted to coke. The carbon deposition rate of the $Rh/La_2O_3/CeO_2–ZrO_2$ catalyst is

**Table 2. Coke Deposition over $Rh/La_2O_3/CeO_2–ZrO_2$ after Acetic Acid Steam Reforming under Various Conditions**

| conditions | mole $C_{(coke)}$ per mole C in acetic acid, % |
|---|---|
| steam reforming $T$ = 750 °C | |
| S/C = 1.5 | 0.025 |
| S/C = 3.0 | 0.009 |
| S/C = 6.0 | 0.006 |
| autothermal steam reforming ($T$ = 750 °C, $O_2$/steam/carbon = 0.15/3/1) | 0.007 |
| steam reforming, time on stream ($T$ = 650 °C, 15 h, S/C = 3.0) | 0.010 |

extremely low. For a steam-to-carbon ratio of 3/1, the amount of coke measured after 3 h of TOS corresponds to an average 0.009% mol of solid carbon formed per mole of converted carbon (from acetic acid). The reduction of the $H_2O/C$ ratio from 6 to 1.5 results in a 4-fold increase in coke deposited, pointing to the importance of steam excess to limit coking. After 15 h of time on-stream, coke deposited on the catalyst amounted to 2.95 wt %, which corresponds to an average percentage rate of coking of 0.010 mol of solid carbon per mole of carbon reacted.

The presence of $O_2$ reduces coke formation by over 20%, but does not fully suppress it. The reason might be related to the fact that the concentration of coke deposited is extremely low and that it limits the beneficial effects of $O_2$. Alternatively, one might hypothesize that the rate of $O_2$ consumption in acetic acid oxidation is much higher than that of the oxidation of any formed carbonaceous deposits. Given that $O_2$ is a limiting reactant (100% conversion), its effect in coking is of minor importance; however, the potential adoption of $O_2$ as a coreactant is a matter of further studies related with the overall energy efficiency and economy of the process.

The above results demonstrate the very low affinity of the catalyst to reactions leading to coke precursor formation or the efficient removal of them from the catalyst surface. The coke deposition rate over $Rh/La_2O_3/CeO_2–ZrO_2$ is 1 order of magnitude lower than the values reported for other catalysts.[39,46] It is well-known that noble metals, especially Rh, form carbon at a substantially lower rate other base metals used in reforming.[13,37]

Both Rh and the support $La_2O_3/CeO_2–ZrO_2$ contribute to the lowering of the carbon deposition rate. The $O_2$ exchange experiments suggest that the presence of $CeO_2$ and the oxygen vacancies that are formed facilitate the diffusion of oxygen atoms through the support. Under steam reforming conditions, the catalyst is in the reduced state, which means that oxygen vacancies are present on the surface of ceria. Even in the absence of gas phase $O_2$, water and $CO_2$ provide oxygen atoms[49–52] by dissociation on the partially reduced oxide surface. The higher the number of oxygen defects, the higher the observed mobility of this atomic oxygen. TPIE experiments with $^{18}O_2$ (see section 3.1) demonstrate the high mobility of lattice oxygen, which is concluded to facilitate the oxidation of coke maintaining the support surface almost clean.

*3.2.4. Characteristics of the Carbonaceous Deposits.* The chemical reactivity of coke deposited on $Rh/La_2O_3/CeO_2–ZrO_2$ has been explored by oxidation of the spent catalysts in a thermo balance. The profiles of $CO_2$ produced from the oxidation of coke on the used catalyst after 3 and 15 h TOS are compiled in Figure 6. The deposits were readily oxidized starting at 200 °C (completion at 350 °C). The duration of the catalytic conversions does not affect the nature of coke because the same oxidation profile was observed after 3 and 15 h time on-stream. The low temperature of oxidation implies that their nature differs from that of aromatic coke, which needs over 500 °C to be oxidized.[53] Takanabe et al. argue that acetone, which is one of the intermediates, is the main source of carbon formation in the acetic acid steam reforming over the $Pt/ZrO_2$ catalyst.[17] Deposited carbon is concluded to exist in the form of oligomers and can be removed by oxygen at temperatures less than 450 °C, in line with the findings of Basagiannis and Verykios for acetic acid reforming on $Ru/MgO-Al_2O_3$.[16] The same quality of carbonaceous deposits (low temperature of removal) was also observed in experiments with the $CeO_2–$


dx.doi.org/10.1021/cs4003063 | ACS Catal. 2013, 3, 1919–1928

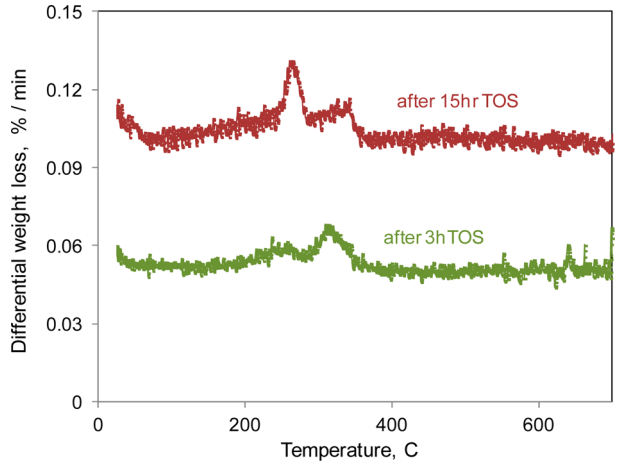


**Figure 6.** Thermogravimetric analysis of used catalyst $Rh/La_2O_3/CeO_2–ZrO_2$in air flow.

$ZrO_2$ support.[37] The similarity between the oxidation profiles of coke from the support alone and from the catalyst containing Rh suggests that the nature of the coke formed was identical in the presence and absence of Rh and that Rh is hardly involved in the oxidation process, indicating that coke is located on the oxide surface.

**3.3. Reaction Scheme.** *3.3.1. Reforming Tests in Transient Mode.* Experiments in transient mode were conducted over the $CeO_2–ZrO_2$ and $Rh/La_2O_3/CeO_2–ZrO_2$. The variations in the concentrations of the products formed together with that of unconverted acetic acid in the gaseous phase are illustrated in Figure 7a,b as a function of temperature. The adsorption of acetic acid on the support starts soon after its admission as its concentration starts decreasing without indication of product formation (Figure 7a). Adsorption continues until the surface is saturated, whereas product formation starts at 220 °C. At the same time, no indication of consumption of mobile acetic acid is provided at least up to 240 °C, implying that the primary products formed derive from adsorbed acetic acid or that a steady state has been reached. The activity starts with the evolution of products, acetone and $CO_2$ originating initially from the adsorbed acetic acid, which undergoes ketonization (eq 1). The ratio of acetone to $CO_2$ being slightly lower than 1 is tentatively attributed to readsorption of a part of acetone on the support, reacting further to $CH_4$, CO, and $H_2$.

$$2CH_3COOH \rightarrow CH_3COCH_3 + CO_2 + H_2O \quad (1)$$

The extent of this reaction is quite large, consuming almost all of the acetic acid up to 450 °C. Acetone declines slowly after this temperature, while the rate of $CO_2$ formation increases. Beyond this temperature, decarboxylation becomes important, leading to $CO_2$ and $CH_4$ (eq 2).

$$CH_3COOH \rightarrow CH_4 + CO_2 \quad (2)$$

In parallel, $H_2$ and CO are formed with steadily increasing rates. The almost 4-fold higher concentration of $H_2$ compared with that of CO indirectly points to the participation of reforming reactions of acetic acid (eqs 3, 4) and other possible intermediates and water gas shift reaction (eq 5).

$$CH_3COOH \rightarrow 2H_2 + 2CO \quad (3)$$

$$CH_3COOH + 2H_2O \rightarrow 4H_2 + 2CO_2 \quad (4)$$

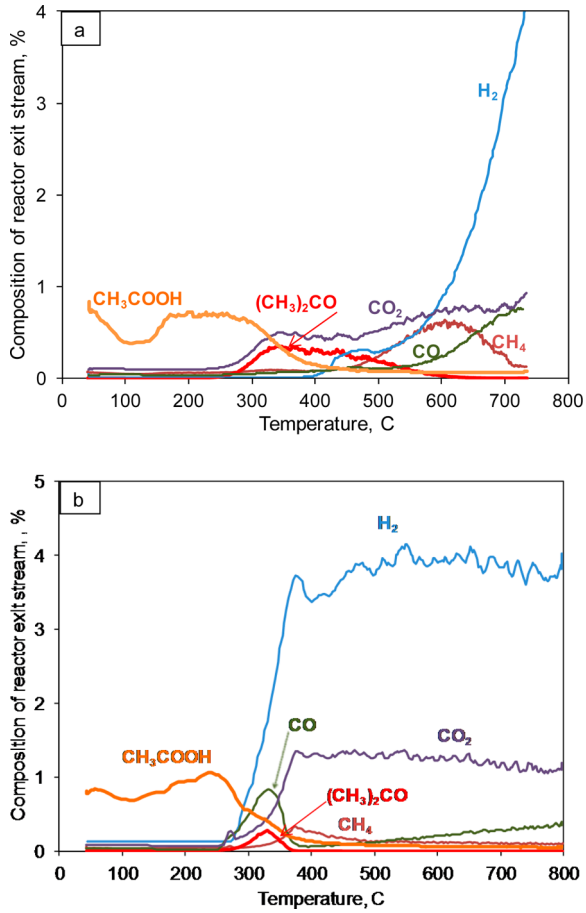


**Figure 7.** Distribution of reactants and products in temperature-programmed reforming reaction of acetic acid over (a) $CeO_2–ZrO_2$ and (b) $Rh/La_2O_3/CeO_2–ZrO_2$catalyst.

$$CO + H_2O \rightleftharpoons H_2 + CO_2 \quad (5)$$

The decreasing concentration of methane after 600 °C, which is associated with the abrupt increase of $H_2$, points to the promotion of reforming reactions at high temperatures. Note that even at the maximum temperature used, 700 °C, the concentrations of $H_2$, CO, and $CO_2$ differed from those at equilibrium under similar conditions (see Figure 3). The ratio of $CO/CO_2$ experimentally observed was around 1, whereas that in equilibrium is 0.5. The deviation from equilibrium is attributed to the low activity of the support to WGS or the transient character of the tests (increase in the reaction temperature with a ramp of 15 °C/min).

With $Rh/La_2O_3/CeO_2–ZrO_2$ (Figure 7b), acetic acid is adsorbed onto the catalyst surface at low temperatures, as also observed with the support. Product formation starts at 250 °C, but the striking difference between the results with the bare support and the catalyst is that $H_2$ production started at 250 °C. The distribution of products in the range from 250 to 370 °C was quite interesting. The evolution of $H_2$, $CO_2$, and $CH_4$ followed the same trend, indicating that all three molecules result from the same intermediate. Their concentration increased drastically up to 370 °C. In the same temperature region, a totally different profile of CO and $CH_3COCH_3$ appeared. Note the sharp peaks of CO and acetone, which maximized at the same temperature of 330 °C. The profiles of CO and acetone showed a maximum at 330 °C and then dropped to almost zero at 370 °C. The similarity of the


dx.doi.org/10.1021/cs4003063 | ACS Catal. 2013, 3, 1919–1928

evolution profiles suggests that these two products originated from the acetic acid that was adsorbed at low temperature ($T$ < 200 °C). Further evidence for the origin of the two products is provided by the carbon balance in this temperature region. The carbon balance at around 330 °C approaches nearly 200%, which means that in this regime, additional carbon is converted (in the form of adsorbed acetic acid), leading to products such as CO and $CH_3COCH_3$.

Thus, steam reforming reactions and water gas shift reactions dominated in the presence of Rh, even at low temperatures, with $H_2$ and $CO_2$ being the main products at temperatures over 350 °C. Further increase in the temperature also favored the formation of CO via the reverse water gas shift. At temperatures over 500 °C, the selectivity to $H_2$ reached almost 100%, demonstrating that reforming reactions of acetic acid and intermediate products ($CH_4$, acetone) dominate. Acetic acid was fully converted at around 400 °C, producing $H_2$ with very high selectivity, in agreement with steady state tests (see Figure 3). In contrast to what was observed with the support, the ratio of $CO/CO_2$ was much lower than that of the equilibrium in the temperature range over 400 °C. The concentration of CO increased steadily with temperature, but remained lower than equilibrium by 60%. The difference might be ascribed to the main role of the metal in driving the reforming and, to a lower degree, of the WGS. In addition, the difference with the steady state tests presented before, in which the $CO/CO_2$ ratio followed the equilibrium composition at 750 °C, is attributed to the transient character of these tests. The fast increase in the reactor temperature (15 °C/min) does not allow the system to equilibrate, as is the case with the steady state tests in which the temperature in the reactor remains constant for over 60 min.

*3.3.2. Mechanistic Considerations.* The differences in the profiles of the products formed over the bare support and the Rh catalyst demonstrate the decisive role of the metal in the reaction pathways. Ketonization dominates only below 250 °C and is especially well catalyzed by redox oxides, such as $ZrO_2$ and $CeO_2$.[54−56] The mechanism as proposed in the literature[57,58] involves the adsorption of the Lewis acid sites of acetic acid on oxygen defect sites of the metal oxides to form the carboxylate. Ketene is formed through abstraction of one of the $\alpha$-H's and formation of $H_2O$. A carboxylate in the proximity reacts further with ketene to form a ketone by eliminating $CO_2$. This is also speculated to occur on $CeO_2$−$ZrO_2$. The absence of ketene in the gas phase products implies that ketene is a surface intermediate readily reacting further. Increasing the temperature above 450 °C shifts the reactions toward decarboxylation, leading to $CH_3$ and $CO_2$ (Figure 7a). The former is rapidly hydrogenated to $CH_4$ on the surface of the support.

In the presence of Rh, the product profiles changed (Figure 7b). $H_2$, $CO_2$, and only traces of $CH_4$ appeared from 250 °C onward, with the rates increasing very fast with temperature. It is speculated that the acetates formed via the dissociative adsorption of acetic acid on Rh form the methyl species that rapidly cleave off further H atoms. The remaining carbon reacts with hydroxy groups of the dissociated $H_2O$, forming $H_2$ and CO as well as $CO_2$ (Scheme 1). Only a small fraction of methyl species is hydrogenated to $CH_4$.

In parallel to this route leading to reforming products, adsorbed acetic acid reacts along a different reaction pathway (Scheme 1). CO and acetone appeared from 250 to 370 °C. The formation of acetone implies that ketonization proceeds, but in this case, the formation of acetone is followed by the

**Scheme 1. Reaction Pathways of Acetic Acid Reforming over $Rh/La_2O_3/CeO_2$−$ZrO_2$ Catalyst**

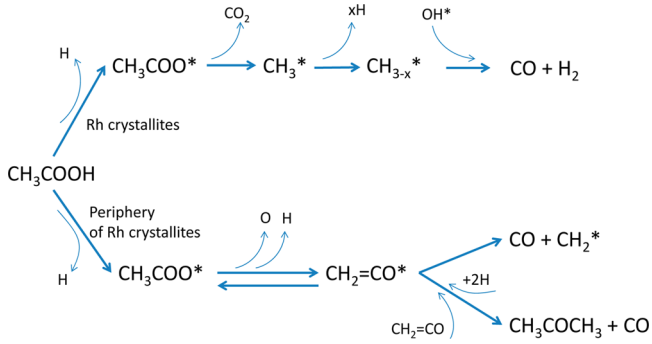


release of CO instead of $CO_2$. This may indicate that the formation of acetone involves the condensation of two ketene molecules rather than of one ketene and one acetate, as suggested for the bare support. This difference may indirectly point to the fact that the active sites of Rh and the support are not identical or that the metal induces a larger concentration of defects, which facilitate the formation of ketenes. The hypothesis is further supported by the much larger concentration of CO compared with that of acetone formed. Note in this context that intermediately formed ketenes not only undergo condensation to acetone, but also decompose to CO and $CH_2$ species, the latter contributing to the pathway of reforming.

Depending on the surface, different adsorbed species are derived from the acids. $CH_3COO^*$ has been reported to be the main species after adsorption of acetic acid on the Pt(111) surface, whereas $CH_3COO^*$ and $CH_3CO^*$ have been observed on Pt(111).[59,60] The distinctively different adsorption structures are likely to determine the pathway leading to CO and $CO_2$ elimination. The formation at low temperatures of CO and $CO_2$ on the Rh catalyst implies the different nature of the sites in which acetic acid has been sorbed, forming $CH_3CO^*$ and $CH_3COO^*$, respectively. Even though direct evidence of the nature of the two sites is not available, we argue that acetate is formed on Rh crystallites, and acetyl is formed on the periphery of the metal particles .

In the previous analysis, we assumed that acetic acid dissociates on the catalyst surface, forming mostly acetates. To verify this, temperature programming reforming of isotopically labeled acetic acid ($CH_3COOD$) was studied on $Rh/La_2O_3/CeO_2$−$ZrO_2$. Apart from $H_2$ and $CH_4$, other differences were not observed among the products, and this is the reason for not including them in Figure 8a, in which the evolution of masses 2 ($H_2$), 3 (HD), and 4 ($D_2$) is illustrated as a function of temperature. As in the case of nonlabeled acetic acid, hydrogen approaches high concentration at temperatures over 350 °C. The appearance of HD indicates that acetic acid dissociated on the surface by the cleaving of O−D bond, forming acetate species and D* (eq 6). The latter combined with H*, deriving either from water dissociation or a methyl group, forms cross-labeled hydrogen molecules HD (eq 7). The direct recombination of D* is negligible, as evidenced from the very weak intensity of the $D_2$ signal.

$$CH_3COOD + 2^* \rightarrow CH_3COO^* + D^* \quad (6)$$

$$H^* + D^* \rightarrow HD \quad (7)$$


dx.doi.org/10.1021/cs4003063 | ACS Catal. 2013, 3, 1919−1928

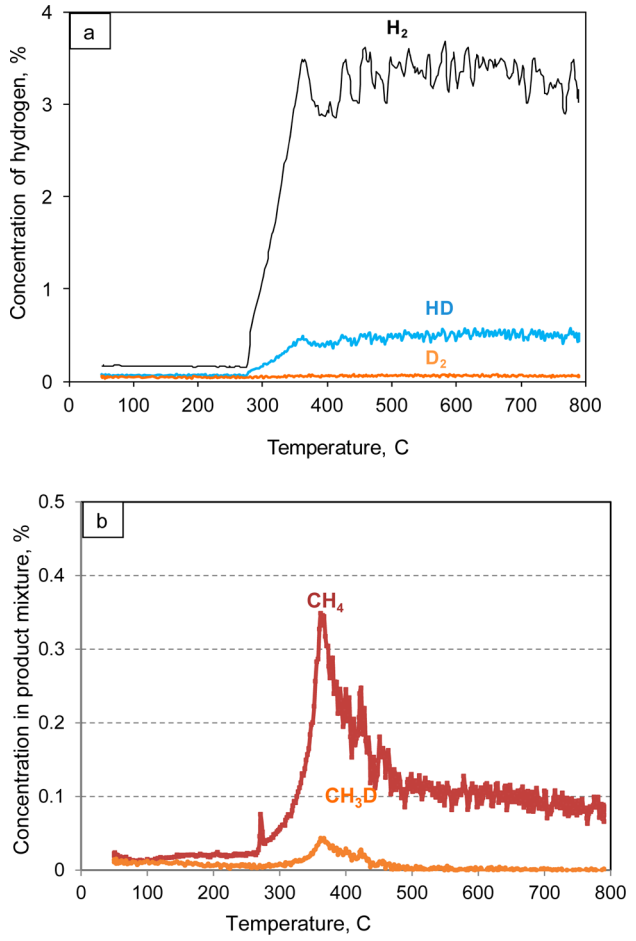


**Figure 8.** Temperature-programmed reforming reaction of isotopically labeled $CH_3COOD$ over $Rh/La_2O_3/CeO_2–ZrO_2$ catalyst. Evolution of (a) hydrogen and (b) methane.

Labeling of methane (Figure 8b) showed apart from mass 16, which corresponds to $CH_4$, mass 17, $CH_3D$. The presence of scrambled methane further supports the evidence of the formation of acetate species and their sequential reaction. These adsorbed species undergo further decomposition at temperature as low as 300 °C to form adsorbed methyl species and $CO_2$ 8.

$$CH_3COO^* \rightarrow CH_3{}^* + CO_2 \quad (8)$$

Methyl species $CH_3$* are a key intermediate in reforming reactions of hydrocarbons and especially of methane.[61] The rate constant of C–H bond scission is considered as the slowest one in the whole reaction sequence. In the case of acetic acid, the fragmentation of the C–C bond, which is more energetically favored than the C–H bond cleavage, leads to the direct formation of the reactive methyl species, in line with conclusions by Guell et al.[62] Once formed, methyl species undergo a series of reactions that are much faster. A methyl group could combine with one OH* and then dehydrogenate to $H_2$ and CO or undergo further dehydrogenations. In addition to the successive dehydrogenations, a small part of the active methyl species could combine with hydrogen species (H or D) to form methane. The presence of $CH_3D$ in the product mixture confirms this pathway (Figure 8b).

The tests with fully deuterium-exchanged acetic acid $CD_3COOD$ provided further information on the participation of water in the formation of products. It is clear from Figure 9a that $H_2$, formed from water decomposition to H* and OH*

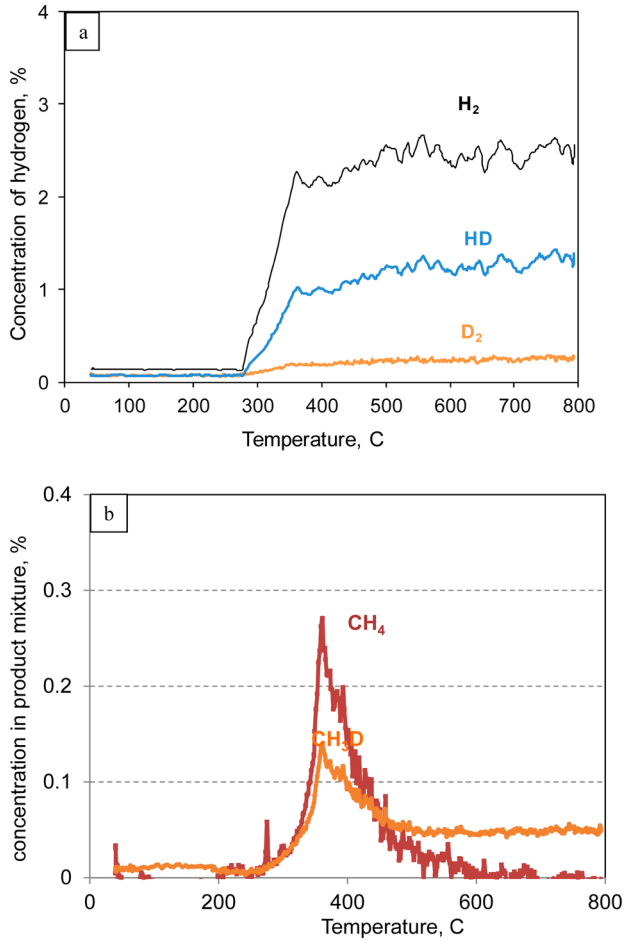


**Figure 9.** Temperature-programmed reforming reaction of isotopically labeled $CD_3COOD$ over $Rh/La_2O_3/CeO_2–ZrO_2$ catalyst. Evolution of (a) hydrogen and (b) methane.

and further recombination of two H*, is the major constituent. The presence of HD indicates that deuterium D* from acetic acid combines with H* from water. The presence of $D_2$ in small proportion in the products further indicates that the formation of $H_2$ can proceed also either via combination of two deuterium atoms derived from dissociative adsorption of acetic acid or from further dehydrogenation of deuterated methyl radicals to methylene radicals and methylidene radicals. Figure 9b provides further evidence for the degree of dehydrogenation of methyl radicals. The presence of unlabeled $CH_4$ and $CH_3D$ in comparable quantities, as with the typical tests, implies that dehydrogenation of methyl species down to atomic C* is possible. Active carbon formed reacts with H* or OH* from water dissociation, forming methane with various isotopic scrambling; however, it cannot be excluded that $CH_4$ and $CH_3D$ can also be formed from partially dehydrogenated deuterated methyl species via exchange of D atoms with H from the surface pool. The presence of $CD_4$ and $CHD_3$ in the products was well-recognized; however, the exact quantification of the signals was not possible because of superposition from other fragments.


dx.doi.org/10.1021/cs4003063 | ACS Catal. 2013, 3, 1919–1928

## 4. CONCLUSIONS

Acetic acid reforming proceeded with high rates (TOF 10 $s^{-1}$ at 550 °C) over 0.5 wt % Rh catalyst supported on $CeO_2$−$ZrO_2$ modified with 3 wt % $La_2O_3$, producing $H_2$ with over 98% selectivity. $CeO_2$ enhances lattice oxygen exchange with the gas phase $O_2$. The oxygen vacancies formed in $CeO_2$ during reforming facilitated the diffusion of atomic O provided via decomposition of steam or $CO_2$. This active oxygen acts as an oxidant for the carbonaceous deposits, contributing thus to the extremely low concentration of coke observed after reforming reactions. The low temperature of carbonaceous deposits oxidation, up to 350 °C, implies that the measured as coke deposits on the surface of $Rh/La_2O_3/CeO_2$−$ZrO_2$ catalyst are oligomers. The $La_2O_3$ modifier stabilizes the catalyst under reaction conditions, as evidenced from the limited loss in the activity in long-term tests (8% after 15 h of TOS). The conversion of acetic acid over the support alone proceeds at >250 °C via a ketonization reaction, whereas at higher temperature, decarboxylation prevails. The overall reaction network is quite complex, with the reforming reactions, however, dominating, even as low as 250 °C, over the catalyst. With the use of deuterated acetic acid, it was proved that on the catalyst surface, acetic acid adsorbs dissociatively at low temperature to acetate and hydrogen. The former carboxylates form methyl species, which undergo further dehydrogenation with intermediate formation of an active carbon reacting with water-derived H and OH. The ketonization reaction is limited to acetic acid molecules adsorbed in the periphery of the Rh crystallites.

## AUTHOR INFORMATION

### Corresponding Author

*Phone: +30 2310 996273. Fax: +30 2310 996184. E-mail: alemonidou@cheng.auth.gr.

### Notes

The authors declare no competing financial interest.

## ACKNOWLEDGMENTS

Angeliki Lemonidou and Ekaterini Vagia acknowledge funding in part from the PENED programme that is cofinanced by E.U.-European Social Fund (75%) and the Greek Ministry of Development-GSRT (25%).

## REFERENCES

(1) Huber, G. H.; Iborra, S.; Corma, A. *Chem. Rev.* **2006**, *106*, 4044−4098.
(2) Bulushev, D. A.; Ross, J. R. H. *Catal. Today* **2011**, *171*, 1−13.
(3) Schoeters, J.; Maniatis, K.; Buekens, A. *Biomass* **1989**, *19*, 129−143.
(4) Kechagiopoulos, P. N.; Voutetakis, S. S.; Lemonidou, A. A.; Vasalos, I. A. *Catal. Today* **2007**, *127*, 246−255.
(5) Sfetsas, T.; Michailof, C.; Lappas, A.; Li, Q.; Kneale, B., J. *Chromatography A* **2011**, *1218* (21), 3317−3325.
(6) Garcia-Perez, M.; Chaala, A.; Pakdel, H.; Kretschmer, D.; Roy, C. *Biomass Bioenergy* **2007**, *31*, 222−242.
(7) Czernik, S.; Bridgewater, A. V. *Energy Fuels* **2004**, *18*, 590.
(8) Vagia, E. Ch.; Lemonidou, A. A. *Int. J. Hydrogen Energy* **2007**, *32* (2), 212−223.
(9) Vagia, E. Ch.; Lemonidou, A. A. *Int. J. Hydrogen Energy* **2008**, *33* (10), 2489−2500.
(10) Wang, D.; Montane, D.; Chornet, E. *Appl. Catal., A* **1996**, *143*, 245−270.
(11) Marquevich, M.; Czernik, S.; Chornet, E.; Montane, D. *Energy Fuels* **1999**, *13*, 1160−1166.
(12) Kechagiopoulos, P. N.; Voutetakis, S. S.; Lemonidou, A. A.; Vasalos, I. A. *Energy Fuels* **2006**, *20*, 2155−2163.
(13) Vagia, E.Ch.; Lemonidou, A. A. *Appl. Catal., A* **2008**, *351* (1), 111−121.
(14) Bimbela, F.; Oliva, M.; Ruiz, J.; Garcia, L.; Arauzo, J., J. *Anal. Appl. Pyrol.* **2007**, *79* (1−2), 112−120.
(15) Basagiannis, A. C.; Verykios, X. E. *Appl Catal., A* **2006**, *308*, 182−193.
(16) Basagiannis, A. C.; Verykios, X. E. *Appl. Catal., B* **2008**, *82* (1−2), 77−88.
(17) Takanabe, K.; Aika, K.; Seshan, K.; Lefferts, L. *Chem. Eng. J.* **2006**, *120*, 133−137.
(18) Rioche, C.; Kulkarni, S.; Meunier, F. C.; Breen, J. P.; Burch, R. *Appl. Catal., B* **2005**, *61*, 130−139.
(19) Takanabe, K.; Aika, K.; Inazu, K.; Baba, T.; Seshan, K.; Lefferts, L. *J. Catal.* **2006**, *243*, 263−269.
(20) Matas Guell, B.; Babich, I.; Nichols, K. P.; Gardeniers, J. G. E.; Lefferts, L.; Seshan, K. *Appl. Catal., B* **2009**, *90* (1−2), 38−44.
(21) Medrano, J. A.; Oliva, M.; Ruiz, J.; Arauzo, J. *Energy* **2011**, *36* (4), 2215−2224.
(22) Wu, C.; Liu, R. *Int. J. Hydrogen Energy* **2011**, *36* (4), 2860−2868.
(23) Larrondo, S. A.; Kodjaian, A.; Fabregas, I.; Zimicz, M. G.; Lamas, D. G.; Walsoe de Reca, B. E.; Amadeo, N. E. *Int. J. Hydrogen Energy* **2008**, *33*, 3607−3613.
(24) Pavlova, S. N.; Sazonova, N. N.; Ivanova, J. A.; Sadykov, V. A.; Snegurenko, O. I.; Rogov, V. A.; Zolotarskii, I. A.; Moroz, E. M. *Catal. Today* **2004**, *91*−*92*, 299−303.
(25) Chen, J.; Wu, Q.; Zhang, J.; Zhang, J. *Fuel* **2008**, *87*, 2901−2907.
(26) Noronha, F. B.; Fendley, E. C.; Soares, R. R.; Alvarez, W. E.; Resasco, D. E. *Chem. Eng. J.* **2001**, *82*, 21−31.
(27) Wang, W.; Stagg-Williams, S. M.; Noronha, F. B.; Mattos, L. V.; Passos, F. B. *Catal. Today* **2004**, *98*, 553−563.
(28) Zhu, T.; Flytzani-Stephanopoulos, M. *Appl. Catal., A* **2001**, *208*, 403−417.
(29) Kusakabe, K.; Sotowa, K.-I.; Eda, T.; Iwamoto, Y. *Fuel Process. Technol.* **2004**, *86*, 319−326.
(30) Rogatis, L.; Montini, T.; Casula, M. F.; Fornasiero, P. *J. Alloys Compd.* **2008**, *451*, 516−520.
(31) Birot, A.; Epron, F.; Descorme, C.; Duprez, D. *Appl. Catal., B* **2008**, *79*, 17−25.
(32) Diagne, C.; Idriss, H.; Kiennemann, A. *Catal. Commun.* **2002**, *3*, 565−571.
(33) Polychronopoulou, K.; Costa, C. N.; Efstathiou, A. M. *Appl. Catal., A* **2004**, *272*, 37−52.
(34) Kundakovic, L.; Flytzani-Stephanopoulos, M. *Appl. Catal., A* **1998**, *171*, 13−29.
(35) Srinivas, D.; Satyaranayana, C. V. V.; Potdar, H. S.; Ratnasamy, P. *Appl. Catal., A* **2003**, *246*, 323−334.
(36) Domine, M. E.; Iojoiu, E. E.; Davidian, T.; Guilhaume, N.; Mirodatos, C. *Catal. Today* **2008**, *133*−*135*, 565−573.
(37) Vagia, E. C.; Lemonidou, A. A. *J. Catal.* **2010**, *269*, 388.
(38) Bouarab, R.; Cherifi, O.; Auroux, A. *Thermochim. Acta* **2005**, *434*, 69.
(39) Basagiannis, A. C.; Verykios, X. E. *Int. J. Hydrogen Energy* **2007**, *32* (15), 3343−3355.
(40) Heracleous, E.; Lemonidou, A. A. *J. Catal.* **2006**, *237*, 175−189.
(41) Boreskov, G. K. *Discuss. Faraday Soc.* **1966**, *41*, 263−276.
(42) Duprez, D.; Descorme, C.; Birchem, T.; Rohart, E. *Top. Catal.* **2001**, *16/17*, Nos.1−4, 49−56.
(43) Sun, K.; Lu, W.; Wang, M.; Xu, X. *Appl. Catal., A* **2004**, *268*, 107−113.
(44) Trovarelli, A. In *Catalysis by Ceria and Related Materials*; Trovarelli, A., Ed.; Imperial College Press: London, 2002, 15−50.
(45) Bedrane, S.; Descorme, C.; Duprez, D. *Appl. Catal., A* **2005**, *289*, 90−96.
(46) Trane, R.; Dahl, S.; Skjoth-Rasmussen, M. S.; Jensen, A. D. *Int. J. Hydrogen Energy* **2012**, *37* (8), 6447−6472.

(47) Chou, T. Y.; Leu, C. H.; Yeh, C. T. *Catal. Today* **1995**, *26*, 53−58.
(48) Ferrandon, M.; Bjornbom, E. *J. Catal.* **2001**, *200*, 148−159.
(49) Koo, K. Y.; Roh, H. S.; Jung, U. H.; Yoon, W. L. *Catal. Lett.* **2009**, *130*, 217−221.
(50) Jun, K. W.; Roh, H. S.; Chary, H. S. *Catal. Surv. Asia* **2007**, *11*, 97−113.
(51) Huang, T. J.; Lin, H. J.; Yu, T. C. *Catal. Lett.* **2005**, *105* (3−4), 239−247.
(52) Laosiripojana, N.; Assabumrungrat, S. *Appl. Catal., A* **2005**, *290*, 200−211.
(53) Rostrup-Nielsen, J. R. In *Catalysis: Science and Technology*; Anderson, J. R., Boudart, M. J., Eds.; Springer-Verlag: New York, 1984.
(54) Rajadurai, S. *Catal. Rev. Sci. Eng.* **1994**, *36*, 385.
(55) Martinez, R.; Huff, M. C.; Barteau, M. A. *J. Catal.* **2004**, *222*, 404−409.
(56) Glinski, M.; Kijenski, J.; Jakubowski, A. *Appl. Catal., A* **1995**, *128*, 209.
(57) Pestman, R.; Koster, R. M.; van Duijne, A.; Pieterse, J. A. Z.; Ponec, V. *J. Catal.* **1997**, *168*, 265−272.
(58) Peng, B.; Yuan, X.; Zhao, C.; Lercher, J. A. *J. Am. Chem. Soc.* **2012**, *134*, 9400−9405.
(59) Gursahani, K. I.; Alcala, R.; Cortright, R. D.; Dumesic, J. A. *Appl. Catal., A* **2001**, *222*, 369−392.
(60) Peng, B.; Zhao, C.; Kasakov, S.; Foraita, S.; Lercher, J. A. *Chem.—Eur. J.* **2013**, *19*, 4732−4741.
(61) Wei, J.; Iglesia, E. *J. Phys. Chem. B* **2004**, *108*, 4094.
(62) Matas Guell, B.; Babich, I.; Seshan, K.; Lefferts, L. *J. Catal.* **2008**, *257*, 229−231.